Applied Chemical Engineering (2026) Volume 9 Issue 1 ISSN: 2578-2010 (O)
doi: 10.59429/ace.v9i1.5881

ORIGINAL RESEARCH ARTICLE

Logical Design, construction, and Computational Characterization of Transition-Metal Complexes Resulting from a Novel Cyclohexenone Ligand

Sarab Alazawi[1,*], Rasha Wali Mohi Al-saedi[1], Wasan M. Alwan[2], Anaam Majeed Rasheed[1], Sinan Midhat AL-Bayati[1]

[1] *Department of Chemistry, College of Science, Mustansiriyah University, Baghdad, 10001, Iraq*

[2] *Department of Chemistry, College of Education for Pure Science (Ibn Al-Haitham), University of Baghdad, Baghdad, 10001, Iraq*

***Corresponding author:** Sarab Alazawi, sarabmahdi@uomustansiriyah.edu.iq

ABSTRACT

Cyclohexenone derivatives have more significant attention in the last current years owing to its varied range of applications in various subject, including medicinal chemistry, materials science, and organic synthesis. A derivative of cyclohexanone was prepared by condensation of chalcone derivative with acetylacetone and ethylacetoacetate to produce new ligands with titles L1 and L2, respectively, via Michael's reaction. The Newly complexes were synthesized by coordination of L1 with transition metals ($CrCl_3$• $6H_2O$, $CuCl_2$•$2H_2O$) and L2 with ($CoCl_2$ • $6H_2O$, $NiCl_2$ • $6H_2O$), and characterized by ^{1}H NMR and LC-MS mass spectral analysis, UV and IR spectroscopy, also the magnetic susceptibility studies, molar conductivity study, C, H, N, and atomic absorption analysis. The results confirmed that both new ligands act as bidentate ligands, coordinating with metal ions through the oxygen atoms of both the ketone and hydroxide groups for L1. In contrast, L2 coordinates through two oxygen atoms of the ketone groups to form complexes with an octahedral geometry. The antibacterial capability of new compound and corresponding metal complexes was investigated against the two kinds of pathogenic bacteria microorganisms (Escherichia còli) and (Stāphylocòccus aureus) compare with the standard drug (Cephalexin), and the results showed that the ligands and their complexes activities ranged from weak to moderately to highly active against the two categories of bacteria compared with the standard drug Cephalexin. Consequently, these complexes show potential as therapeutic agents and may emerge as strong competitors to currently available pharmaceuticals. A comprehensive theoretical investigation of the ligand and its metal complexes was conducted by density functional theory (DFT) at the B3LYP level with the 3-21G basis set to provide a consistent correlation with the experimental findings, and shows that L2 and corresponding complexes are more stable compared with L1and its complexes. L2 and its complexes exhibit the highest energy gaps and chemical hardness, confirming their kinetic stability and reduced reactivity compared to other complexes.

Keywords: cyclohexenone derivatives; michael addition; theoretical study; antibacterial

ARTICLE INFO

Received: 8 January 2026
Accepted: 25 February 2026
Available online: 24 March 2026

1. Introduction

Cyclohexenone derivatives, a class of compounds widely known for their various chemical properties, have been focal substantial attention in both the fields of organic synthesis and coordination chemistry. These derivatives have confirmed to be highly useful and have found applications in various areas of the chemical industry[1]. Functionalization of the cyclohexenone ring system has been done by several approaches: introducing substituents on the ring of cyclohexenone and different functional groups. These changes not only to improve the reactivity of the cyclohexenone derivatives but also lead

to produce of new and interesting coordination complexes[2]. Michael addition of ethyl acetoacetate to chalcone is one of the primary synthesis routes to obtain cyclohexenone derivatives, producing 4,6-diaryl-2-oxocyclohex-3-ene-1-carboxylate derivatives. These compounds represent as efficient method for produced merged isoxazoles, pyrazoles, and quinazolins. By this approach, several cyclohexenone derivatives have been already synthesized and characterized[3,4].

In extension of the previous study of 4,6-diaryl-2-òxò-cyclòhex-3-ene-1-carboxylates, as a novel cyclohexenone derivatives were resulting from 6-methoxy-2-naphthylaldehyde. This study including the creation, characterization, and antimicrobial properties of these compounds extensively investigated. Of particular interest the series is ethyl4-(4-chlorophenyl)-6-(6-methoxy-2-naphthyl)-2-oxòcyclohex-3-ene-1-cārboxylate, which has been fully characterized through single crystal studies[5].

Complexes of cyclohexenone derivatives have been extensively studied due to their potential in forming stable complexes with metal ions. Among these metal ions, copper (II) ion has shown remarkable reactivity and complexation properties with cyclohexenone derivatives which has displayed fascinating structural features and attracting the scientists around the world.

Furthermore, cyclohexenone-Cu2+ complexes have shown potential applications in catalysis, sensing, and material science[6]. Number of these compounds have been explored for their abilities as catalyze in organic reactions, such as oxidation, reduction, and cross-coupling reactions. Besides, this has unique properties of the complexes render them ideal candidates for sensing applications as they can exhibit selective and sensitive response toward specific analytes, including metal ions or biomolecules.

Besides catalysis, the metal complexes of cyclohexenone derivatives have been found to act with promising results as antimicrobial agents. These specific structures together with coordination can result in enhanced bioactivity, making them effective against resistant strains of bacteria and fungi. This opens up new possibilities for developing novel antimicrobial agents that could help in tackling the growing threat of antibiotic resistance[3]. The aims of this study to synthesize and characterize cyclohexenone derivatives in orderto investigate their complexation behavior with transition metal ions.in order to identify novel coordination complexes with enhanced reactivity and selectivity in various chemical transformations. Also, to investigate the theoretical study for the ligands and its complexes. The unique structural diversity and functional characteristic of the cyclohexenone-metal complexes are likely to be very beneficial to development of pharmaceuticals.

2. Materials and methods

2.1. Materials

Chemical materials were supplied in the highest purity and were utilized as received, all of which were sourced from Fluka, Aldrich, BDH, and Merck Companies without any additional purification. We used (ethylaceto acetate, acetylaceton,97% purity, Sigma-Aldrich, USA), ($CrCl_3.6H_2O$, $NiCl_2.6H_2O$, $CoCl_2.6H_2O$ and $CuCl_2$. $2H_2O$, Sigma-Aldrich, USA), (, N, N-Dimethyl Formaide (DMF) and Chloroform,99.98% purity, BDH, UK), (Dimethyl sulfoxide,99.5% purity, Sigma-Aldrich, USA), (Dichloro methane,99.5%, Merck, Germany), (Glacial acetic acid,100% Purity, Mêrck,Germany) and (Ethanol absolute,99% purity, Merck, Germany).

2.2. Instrumentation

The determination of melting points for the ligand and the synthesized complexes by (SMP30 apparatus), and the elemental analyses (C.H.N.) were found by utilizing (C.H.N.S) Italy Eurovector instruments and software. The ratio of metal transitions of the prepared complexes was estimated using a flame atomic absorption spectrophotometer (Shimadzu-670 AA). As well as the data of infra-red spectra were assigned by

using the device FT-IR-8300 Shimadzu of range (4000 - 200) cm-1, and the sample discs were prepared in (CsI) for the complexes only, and the ligand was estimated by Bruker Alpha II range (4000- 400) cm-1. The determination of susceptibilities measurements of samples at its solid state was achieved by Faraday's method by using the apparatus (Balance Magnetic Susceptibility Modal MSB-MKI); themolar conductivity of the complexes was measured exploitation electrolytic conductivitydevice (model WTW conductivity photometer series 82362 Weillhium); the Platinum electrode of the device is type (EDC 304); the constant of cell is (1cm), and the concentration is ($1*10^{-3}$M) and DMSO is used as a solvent is at 25°C. Electronic spectra were found by using the apparatus (UV-visible spectrophotometer Varian) at 25 °C. With ($1*10^{-3}$M) concentrations for all prepared ligand and complexes, in DMSO. A Shimadzu GC-MS Ultra QP2010 was used to record GC-MS data for the ligand. The LC-MS measurement for complexes was recorded by (An IC/MS-MSAB Sciex model Q-Trap 3200) in Basra University / College of Science. NMR spectra measurements were carried out using a400 MHz spectrometer for ^{1}H NMR and a100 MHz spectrometer for ^{13}C NMR, both from Varian. The experiments were performed in DMSO-D_6, using tetramethylsilane (TMS) as an internal standard. The study of the biological activity was done in the laboratories of Mustansiriyah University / College of Science / The Department of Biology.

2.3. Preparation of ligands

A. Preparation of chalcon derivative[7]

KOH solution (5 mL of a 40%) was added to a thoroughly stirred solution of 4-bromobenzaldehyde (1.2g, 6.4 mmol) and 4-bromoacetophenone (1.48g, 7.6 mmol) in 25 mL of methanol. After stirring the reaction mixture for the entire night, the separated yield product was obtained and filtered. Methanol was used to recrystallize the finished product.

B. General procedure for preparation of Cyclohexenone derivatives (L1, L2)[8]

A solution of acetylacetone (1.48 ml, 1.48 mmol) or ethylacetoactate (0.2g, 1.6mmol) in sodium hydroxide solution (10% NaOH) was stirred for one hour at room temperature. (**Figure 1**)

After adding the chalcon derivatives (0.4g, 1.2 mmol), the mixed solution was stirred. The reaction mixture was then dumped onto cold hydrochloric acid after being refluxed for twelve hours. After filtering off the solid product, it had been washed with water, dried, and recrystallized from methanol.

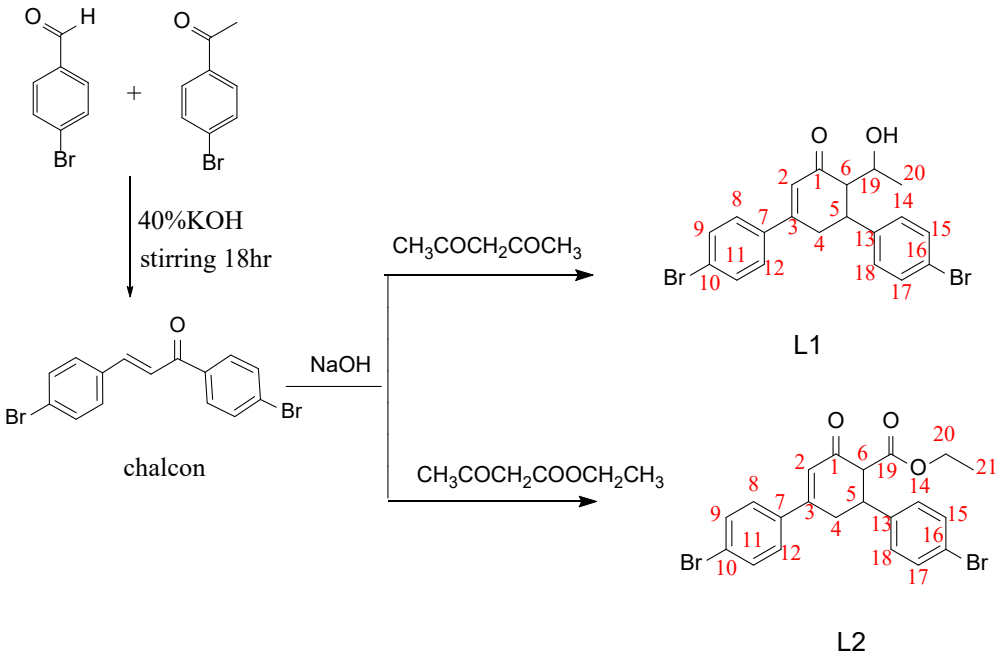

Figure 1. The synthesis route of ligands (L1, L2).

2.4. Preparation of complexes

Ethanolic solution of metal ion salts $CrCl_3.6H_2O$ (0.03g, 1mmol), $NiCl_2.6H_2O$ (0.02g, 1mmol), $CoCl_2.6H_2O$ (0.02g, 1 mmol), and $CuCl_2.2H_2O$ (0.02 g, 1mmol), respectively, was added to ligand L1 or L2 (0.05 g, 2 mmol) which was dissolved in ethanol in the ratio of 2:1, with stirring (**Figure 2**). A mixture was heated under reflux for two hours. After forming a dark green precipitate, it was filtered out, repeatedly cleaned with hot ethanol, and recrystallized in methanol. The physical data of the synthesized complexes are depicted in **Table 1**.

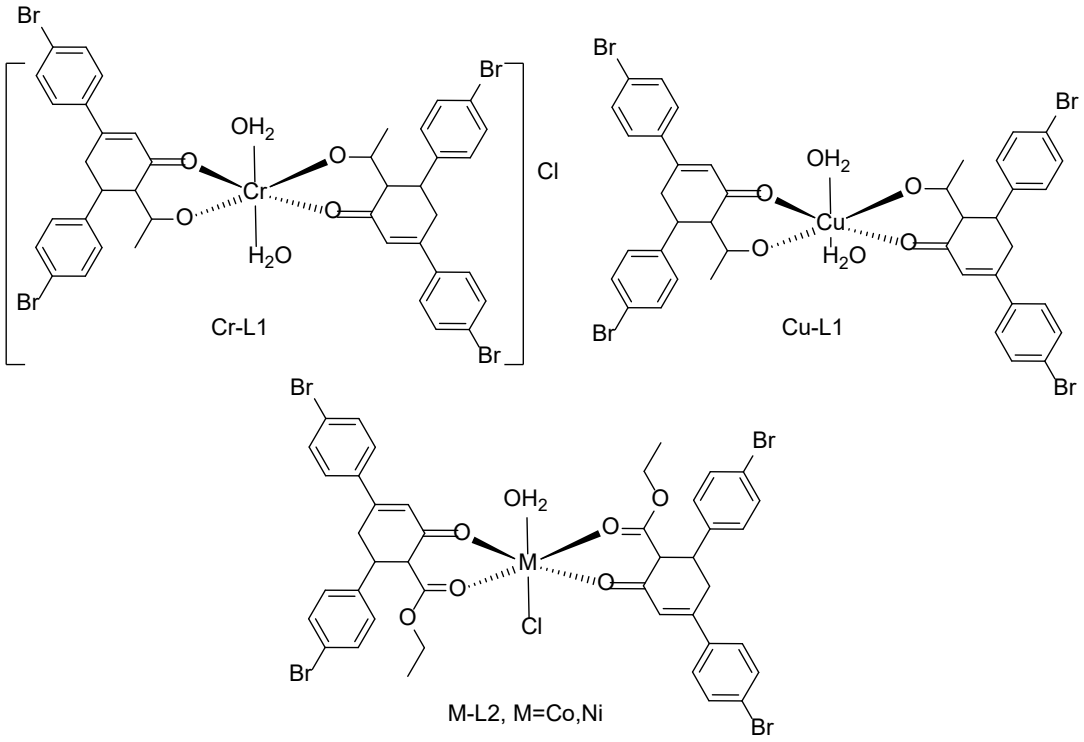

Figure 2. The structure of L1, L2 complexes.

Table 1. Physical characteristics of synthesized ligands and their complexes.

Complexes	M.P(C°)	Color	Yield%	C % Theoretical (Practical)	H% Theoretical (Practical)	N% Theoretical (Practical)	%M Theoretical (Practical)
L1	132 C°	White	85%	59.21 (58.7)	4.47 (4.80)	-	-
$Cu(C_{20}H18Br_2O_2)_2.2H_2O$	>300C°	Dark Brawn	80%	52.74 (52.3)	4.43 (4.9)	-	6.98 (6.54)
$Cr(C_{20}H18Br_2O_2)_2.2H_2O$	>300 C°	Dark Green	75%	48.65 (48.21)	4.49 (5.01)		10.53 (10.11)
L2	158 C°	White	80%	63.17 (63.58)	4.80 (4.55)	-	-
$Ni(C_{20}H_{18}Br_2O_2)_2.2H_2O$	>300 C°	Light yellow	75%	52.26 (52.69)	5.22 (5.05)	-	6.08 (5.65)
$Co(C_{21}H_{18}Br_2O_3)_2.2H_2O$	>300 C°	Grey	70%	52.24 (51.96)	5.22 (5.63)	-	6.10 (5.66)

2.5. Computational study

Gaussian 09 software was used for all theoretical calculations. By employing the B3LYP functional with the 3-21G basis set for generating vibrational frequency calculations through gradient-corrected DFT[9]. For the metal ions, the SDD method was applied. For the C, H, O, N, Br, and Cl atoms, the Pople-style 3-21G basis set was used. The optimized ground state geometries correspond to their true minima on their potential energy surfaces, which were confirmed by the presence of only absolute frequencies. To elucidate their molecular orbital properties, a simulation of the computed HOMO and LUMO energy levels, electronic properties, and the molecular electrostatic potential (MEP) were also considered. Additionally, the energies of the frontier HOMO and LUMO were utilized to estimate chemical softness and hardness, as well as other physical properties, which provide essential information about the molecule's chemical characteristics and reactivity. Lastly, these computational findings were compared with experimental results to assess their accuracy.

3. Results

3.1. Electronic spectra Study of ligands and their complexes

Ligand standard solutions and their complexes were prepared at a concentration of 1×10^{-3} using an ethanol solvent and measured at room temperature using a UV-visible spectrometer. Two types of transitions appeared for both ligands L1, namely (π→ π*) and (n → π *) at (222 nm, 313nm,) and L2 (229nm, 310nm) respectively. L1-Cu (II) complex's electronic spectra that exhibited two peaks of absorption. The first peak was observed at (401 nm) and the second peak was observed at (505 nm) indicated to the transitions $^2B_1g \rightarrow {}^2Eg$ and $^2B_1g \rightarrow {}^2B_2g$, which confirm the octahedral shape surrounding Cu (II) metal ion. Cr (III) complex's electronic spectrā illustrates the bands in the areas (425 nm), (549 nm) and (612 nm) due to the $^4A_2g(F) \rightarrow {}^4T_2g(F)$ (1) and ^4A_2g (F)→^4T_1g (F) (2) and ^4A_2g (F)→^4T_1g(P) (3) and have spin allowed. These transitions are characteristic of an octahedral coordination environment around the Cr (III) center[10]. While the (L2-Co) complex shows three bands at (358nm), (420nm), and (510nm), which might be attributed to $^4T_1g \rightarrow {}^4T_2g$ (Ƒ), $^4T_1g \rightarrow {}^4T_2g$ (Ƥ), and $^4T1g \rightarrow {}^3A_2g$(Ƒ), subsequently, which are suggested the octahedral structure around Co(II) metal ion[11]. L2-Ni complex's electronic spectra exhibited three spin allowed peaks at (373nm), (420nm), and (512 nm) respectively, indicating the transitions $^3A_2g(F) \rightarrow {}^3T_2g$(Ƒ)(ν1), $^3A_2g(F) \rightarrow {}^3T_1g$(Ƒ)(ν2) and ^3A_2g(Ƒ) → $^3T_2g(F)$(ν3), it was found typical of Ni (II) in octahedral form[12]. As shown in **Figure 3**.

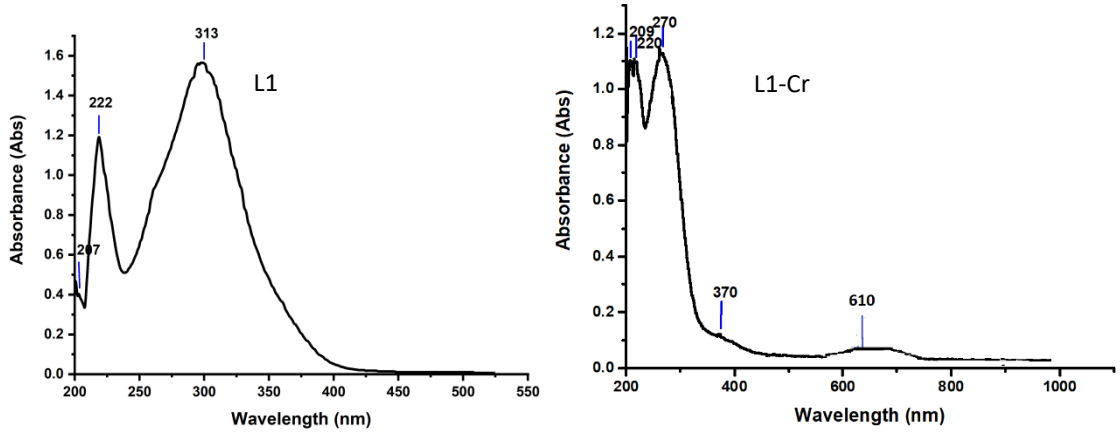

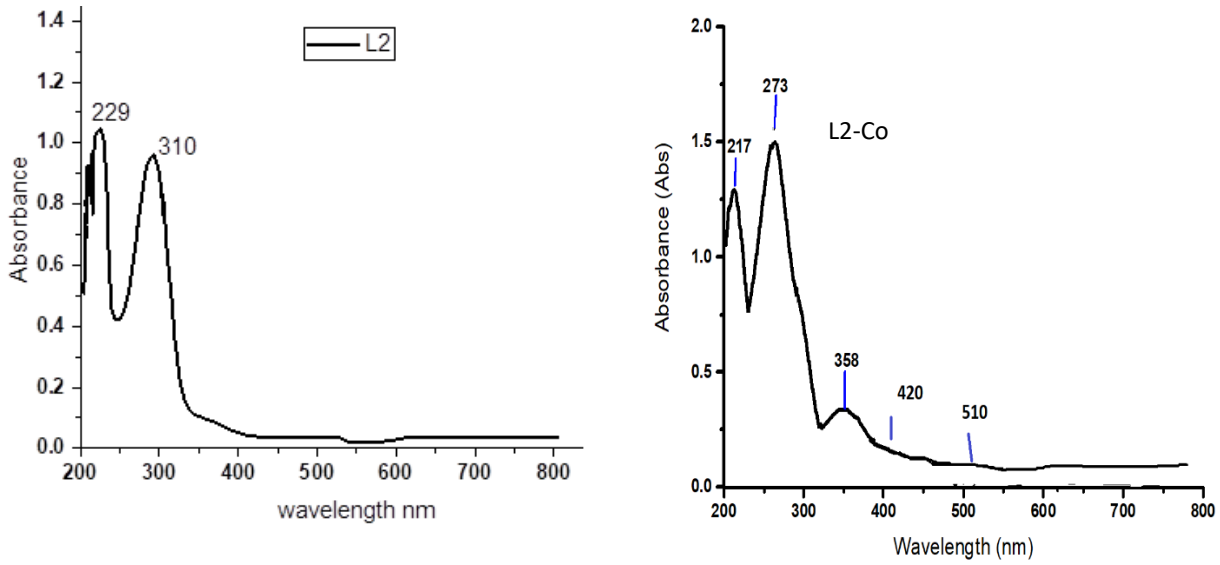

Figure 3. The Uv-Vis spectra of L1, L2, and their complexes.

Table 2. Uv-Vis spectra and molar conductivity and magnetic moment of L1, L2 and their complexes.

Compound	Band peak (nm) (theoretical)	Electronic transition	Suggested structure	Molar Cond. $S.cm^2.mol^{-1}$	μeff. (B.M)
L1	222(213) nm 313(296) nm	π→π* n→π*	------	------	------
L1-Cu	401(409) nm 505(495) nm	$^2B_1g \rightarrow {}^2Eg$ $^2B_1g \rightarrow {}^2B_2g$	oh	9	1.74
L1-Cr	425(445) nm 549(565) nm 610(612) nm	$^4A_2g(F) \rightarrow {}^4T_2g(F)$ $^4A_2g(F) \rightarrow {}^4T_1g(F)$ $^4A_2g(F) \rightarrow {}^4T_1g(P)$	oh	75	3.89
L2	229(210) nm 310(295) nm	π→π* n→π*	------	-----	-----
L2-Co	358(367) nm 450(438) nm 510(528) nm	$^4T_1g \rightarrow {}^4T_2g$ (F) $^4T_1g \rightarrow {}^4T_2g$ (P) $^4T_1g \rightarrow {}^3A_2g(F)$	oh	8	4.85
L2-Ni	373(375) nm 420(418) nm 512(520) nm	$^3A_2g(F) \rightarrow {}^3T_2g(F)$ $^3A_2g(F) \rightarrow {}^3T_1g(F)$ $^3A_2g(F) \rightarrow {}^3T_2g(F)$	oh	11	2.94

3.2. FT-IR spectra of Ligands (L1, L2) and its complexes

The IR spectra of ligands compared with IR spectra of their complex use to investigate the inorganic connection position of the ligands with the metal ions in the areas between 4000 - 400 cm-1 using a CsI disc (**Table 3**). Both L1 and L2 ligands, and their complexes were used as solids. Ligand L1 showed transitions in the IR region that appeared at (3398cm-1) (**Figure 4**). For the assignment to -OH, while (L1-Cu) complex showed the absence of these transitions and instead a new band is seen at (516 cm-1), attributed to M-O transition, and (531 cm-1) for L1-Cr, also the band at (1655cm-1), attributed to C=O, in **Figure 5, 6**. IR spectrum of ligand L2 showed a band at 1732 cm-1, indicating to the (C=O) ester group and a band at 1655 cm-1, indicating to the (C=O) of the aromatic ring (**Figure 7**), IR spectra of (L2-Co) complex and (L2-Ni), showed that the (C=O) band of the aromatic ring shifted towards the high frequencies, as well as the group (C=O) shifted towards the high frequencies for L2-Co while L2-Ni shifted to, which is evidence for its consistency with the central metal ion. Also, another peak was observed at 533cm-1 and 540 cm-1, respectively,

which further confirms the connection of the ligand and metals via the oxygen atoms[13,14] as shown in **Figure 8**. The results of the theoretical study are in excellent consent with the experimental results.

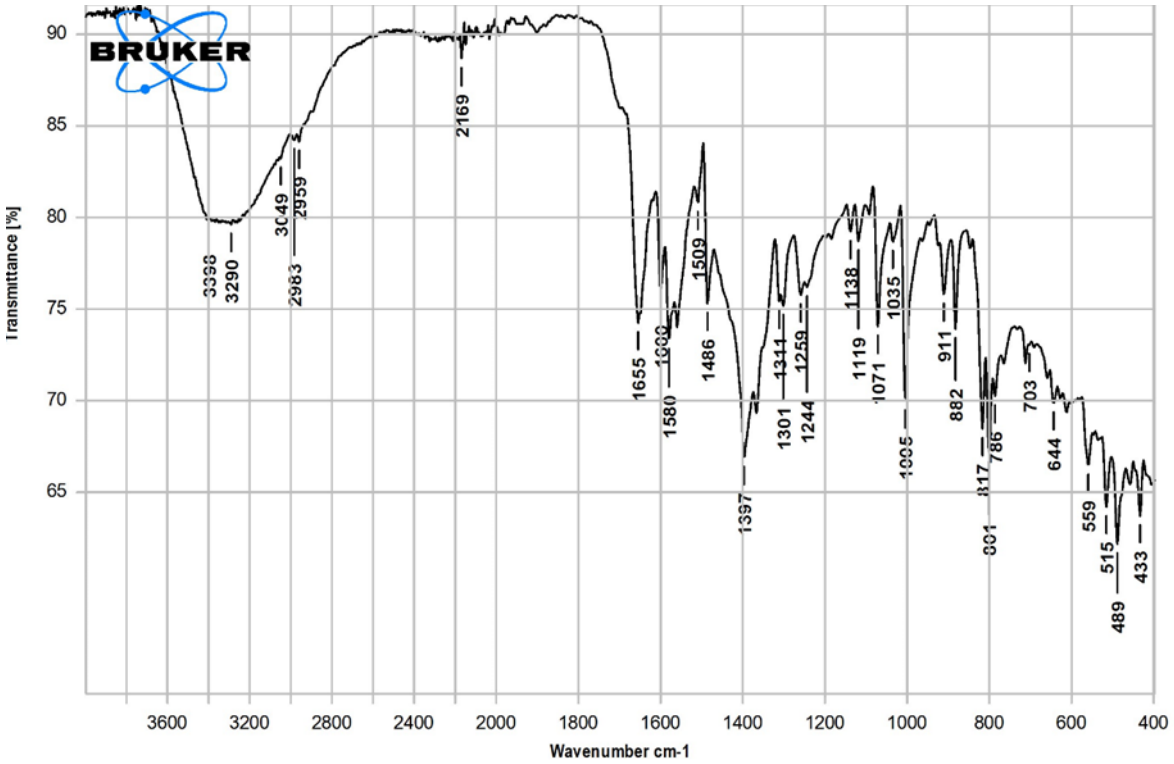

Figure 4. IR spectrum of L1.

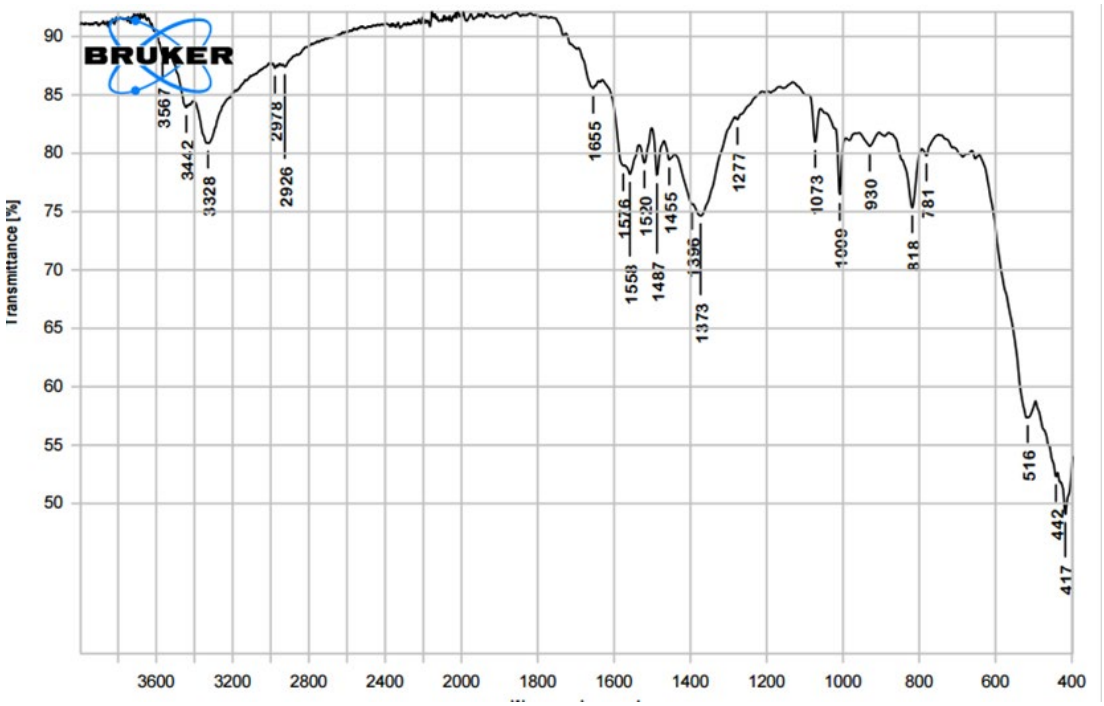

Figure 5. IR spectrum of L1-Cu.

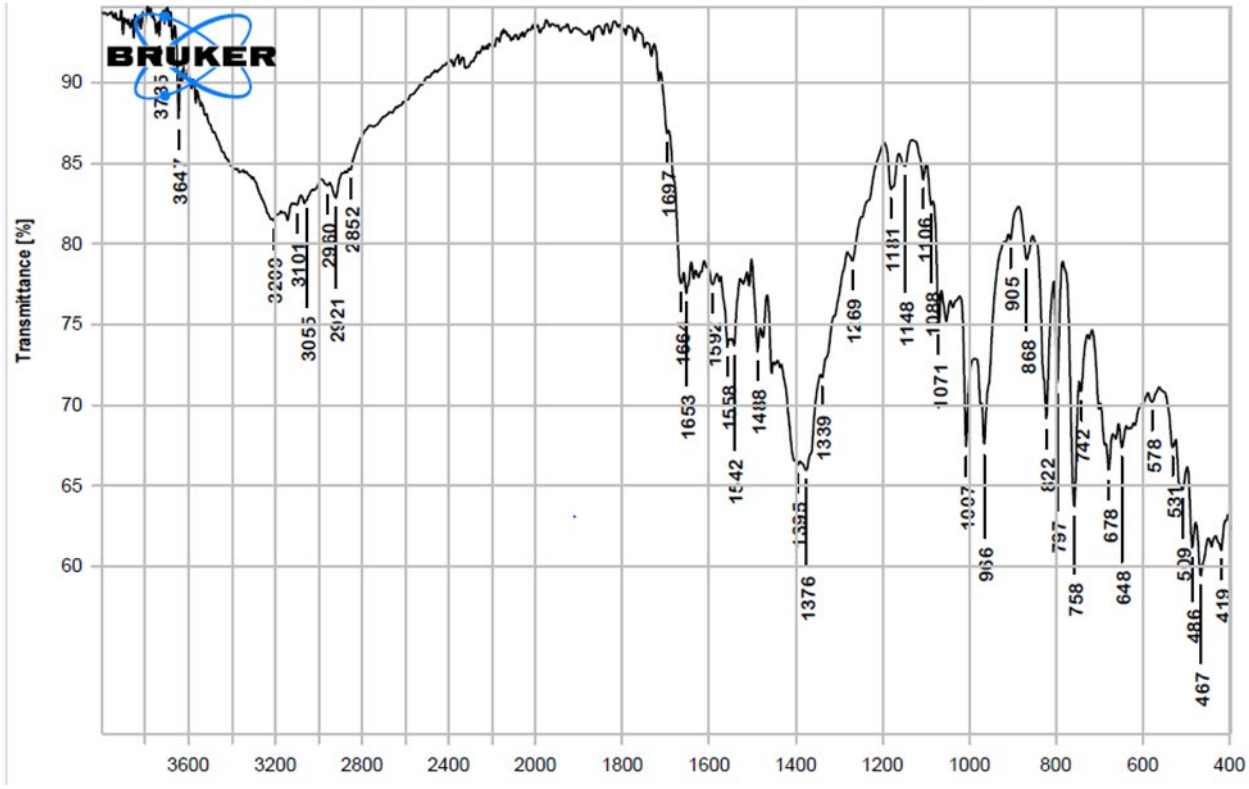

Figure 6. IR spectrum of L1-Cr.

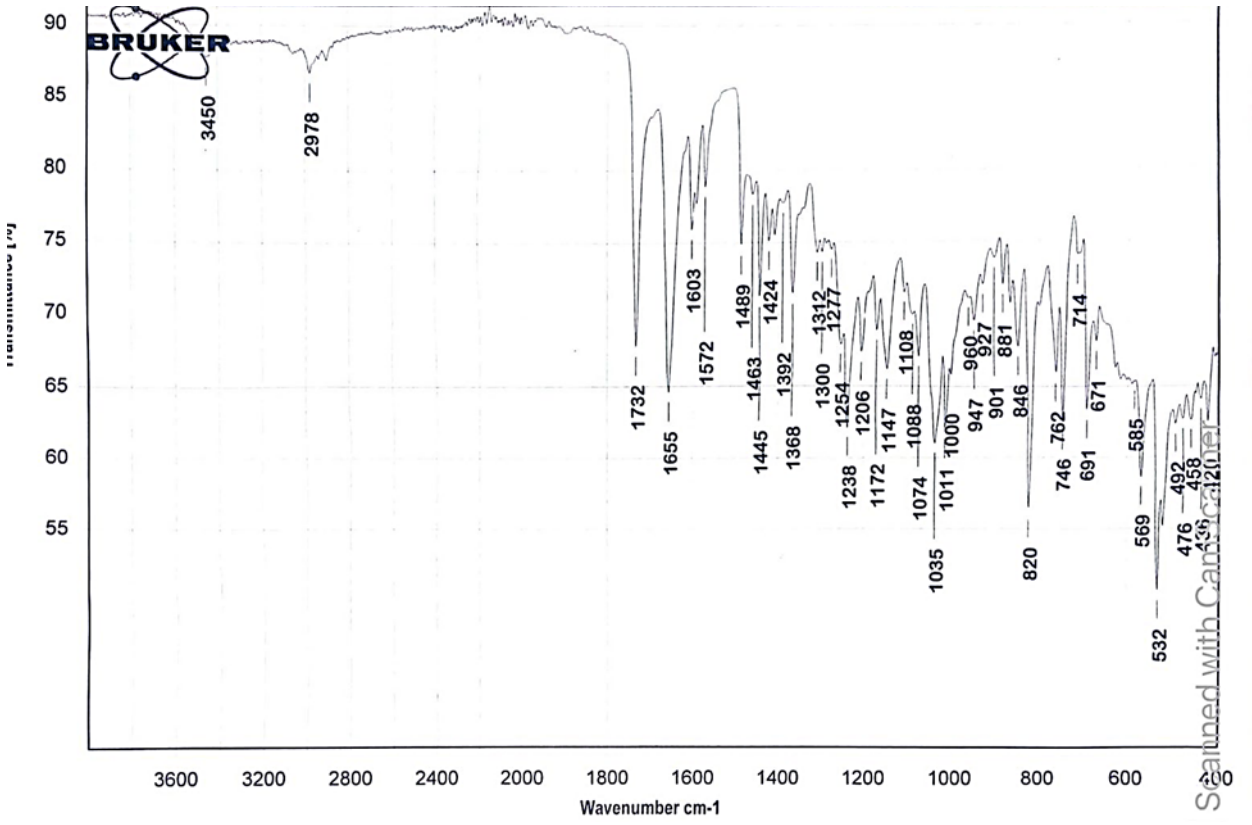

Figure 7. IR spectrum of L2.

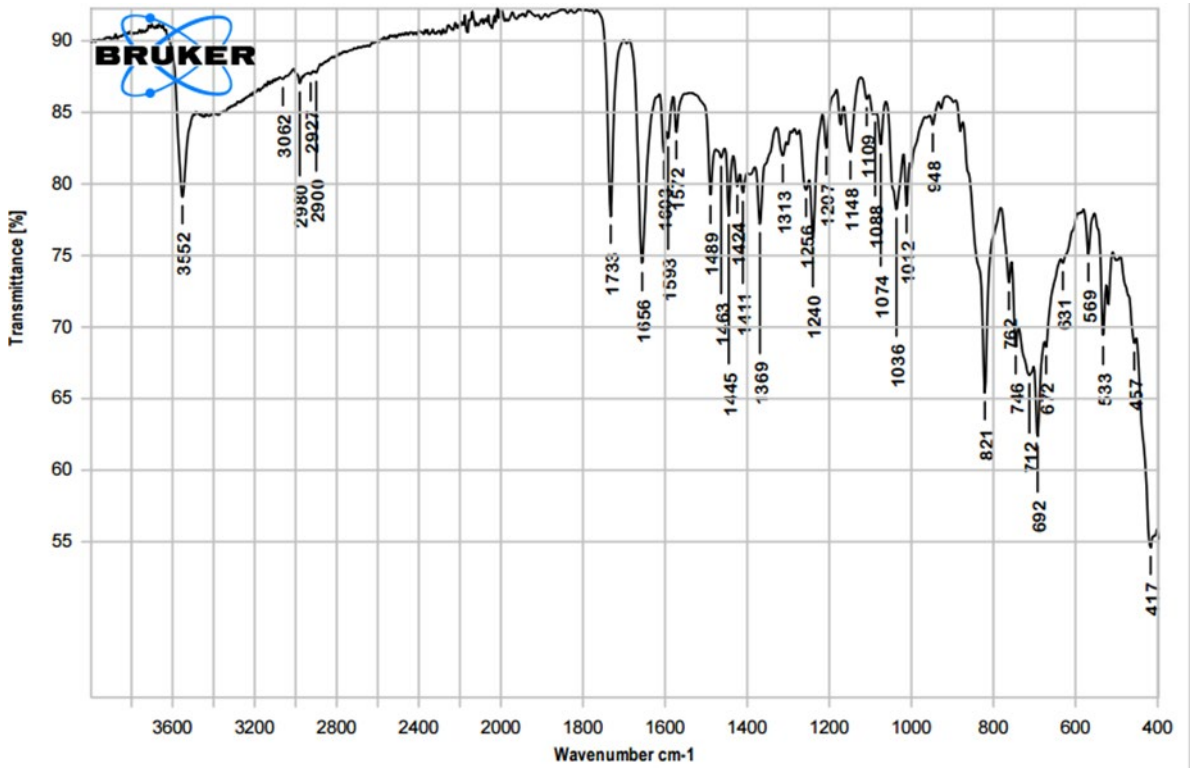

Figure 8. IR spectrum of L2-Co.

Table 3. IR spectra of ligands L1, L2 and its complexes in cm^{-1}.

Compound	ν-C=O ester(theoretical)	ν-C=O ring (theoretical)	νC-OH (theoretical)	νOH (theoretical)	M-O (theoretical)	M-Cl
L1	------	1655(1673) cm^{-1}	1301(1325)	3390(3546) cm^{-1}	-----	-----
L1-Cu	------	1654(1655)	1319(1322)	-----	516(521)	---
L1-Cr	-----	1653(1644)	1376(1376)	----	531(529)	
L2	1732	1655(1489)	----	----	------	
L2-Co	1733(1626)	1656(1619)	-----	-----	533(497)	(473)
L2-Ni	1734(1654)	1630(1636)	-----	-----	540(443)	(467)

3.3. Magnetic Susceptibility and Conductivity Measurement

The structure of the complexes was determined by combining the molar conductivity data with the magnetic susceptibility results. The effective magnetic moment (μeff) data were determined in ethanolic solution at room temperature for the complexes with concentration (10-3M) and are listed in **Table 2**. The Cu-L1 complex's practical magnetic moment value was 1.92 BM, indicating a distorted octahedral shape[14]. The magnetic moment for Cr-L1 was found to be about 3.89 BM, indicating the presence of three unpaired electrons. The value of molar conductance (75 s cm^2 mol^{-1}) confirmed that the complex has an electrolyte behavior (**Table 2**). Within the expected range of octahedral configuration, the computed value of the Co-L2 complex's effective magnetic moment was observed at (4.65) B.M. While the magnetic moment value of the Ni-L2 complex was (2.94) B.M., An octahedral shape surrounding Ni (II) was confirmed by the ligand field characteristics. The values of molar conductance of Co (II), Ni (II), and Cu (II) complexes were (8, 11, and 9 s. cm2Mol-1), respectively, indicating a non-electrolyte nature.

3.4. Nuclear Magnetic Resonance Data of ligands and their complexes

The [1]HNMR spectra of the newly synthesized ligands L1 and L2 recorded in DMSO-d6 at room temperature shows the same peak as following: a doublet signal with two integrals at (7.84ppm), (7.70ppm), (7.68 ppm) and (7.36ppm) attributed to protons with number (8,12), (9,10), (17, 15) and (14,18) respectively. Also, a multiple peak with one integral was observed at (6.25ppm) of L1 and (6.26ppm) of L2, indicating the proton (2). It can also recognize a doublet peak at (3.35ppm) in the L1 spectrum assigned to the proton of (OH). At the same time, L2 does not shows this peak instead a multiple peak with two integrals at (3.87ppm) indicted to proton (20), in addition, a doublet peaks at (1.34ppm) was assigned to the three protons of methyl (20) in L1, whereas L2 spectrum shows this peak as a triplet at (2.95ppm) referring to protons of methyl group (21). The NMR spectra of the complexes show the same peaks, shifted to higher fields, and the proton of the (OH) group disappears in all L1 complexes as a result of coordination with the metal. [13]C NMR spectra of ligand L1, L2 exhibited the same peaks at (C1)200, (C3)154, (C13) 141, (C7)136, (C4) (C5) 132, (C2), (C8), (C12) 127, (C10) (C16) 122, (C6) 64, (C4)36, (C5)34, (C20)21. The only difference observed between L1 and L2 is that the peak of (C19) was observed at (63) in L1 and at (170) in L2. In addition, a new peak was observed in the spectra of L2 at (61 and 14), attributed to (C20) and (C21) respectively, but not found in the spectra of L1. As shown in **Figure 9, 10, 11, 12**.

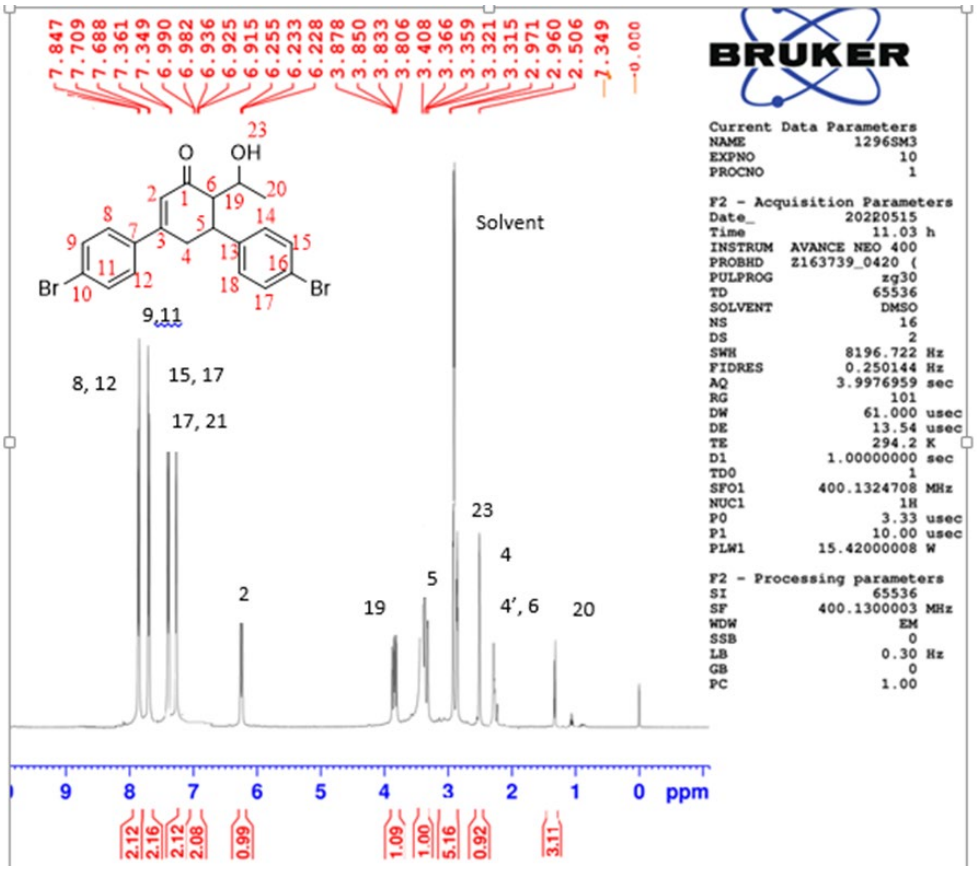

Figure 9. [1]HNMR spectrum of L1.

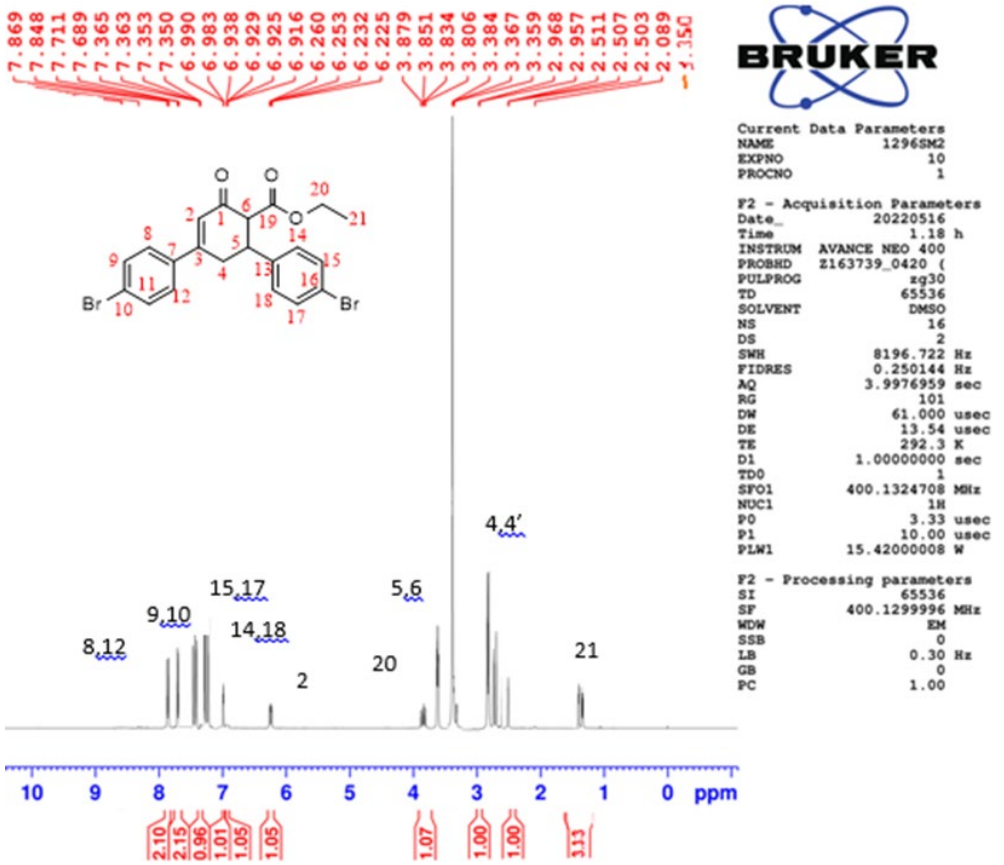

Figure 10. [1]HNMR spectrum of L2.

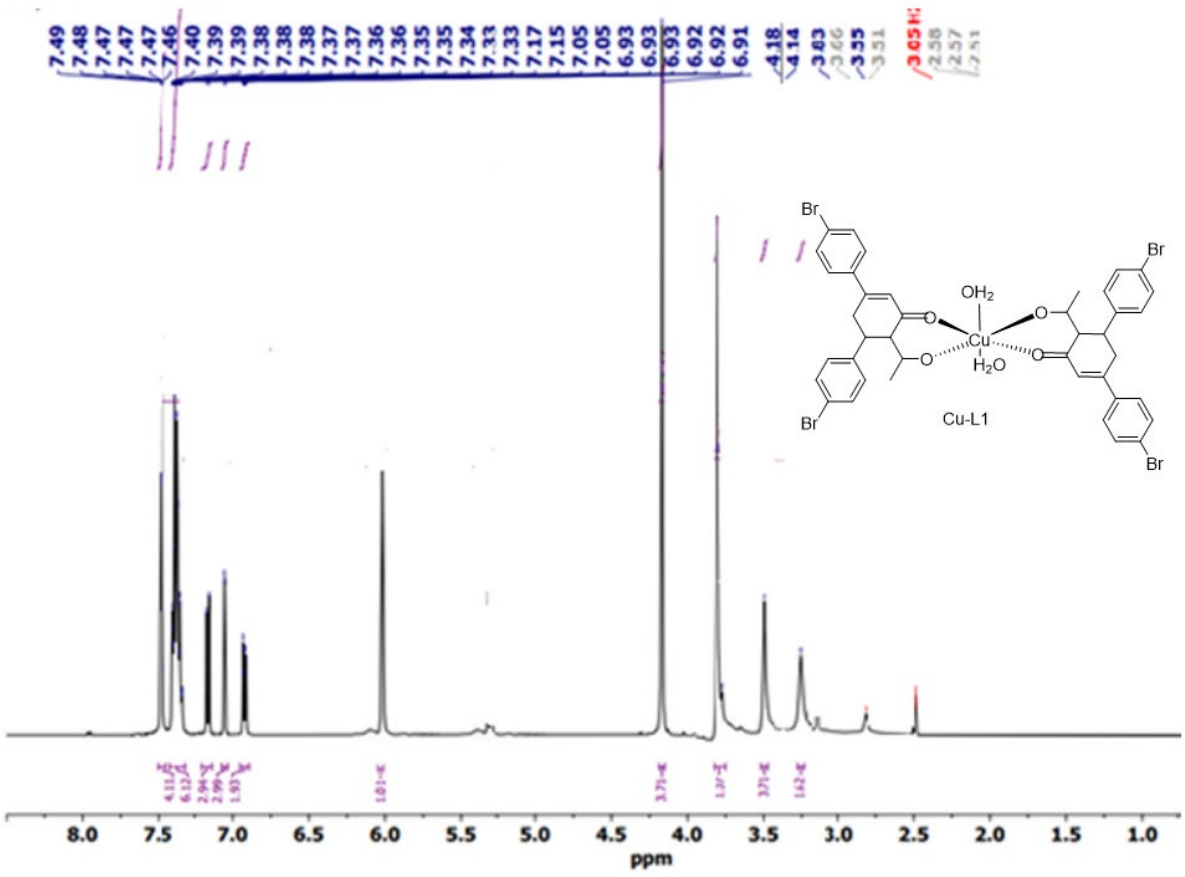

Figure 11. [1]HNMR spectrum of L1-Cu.

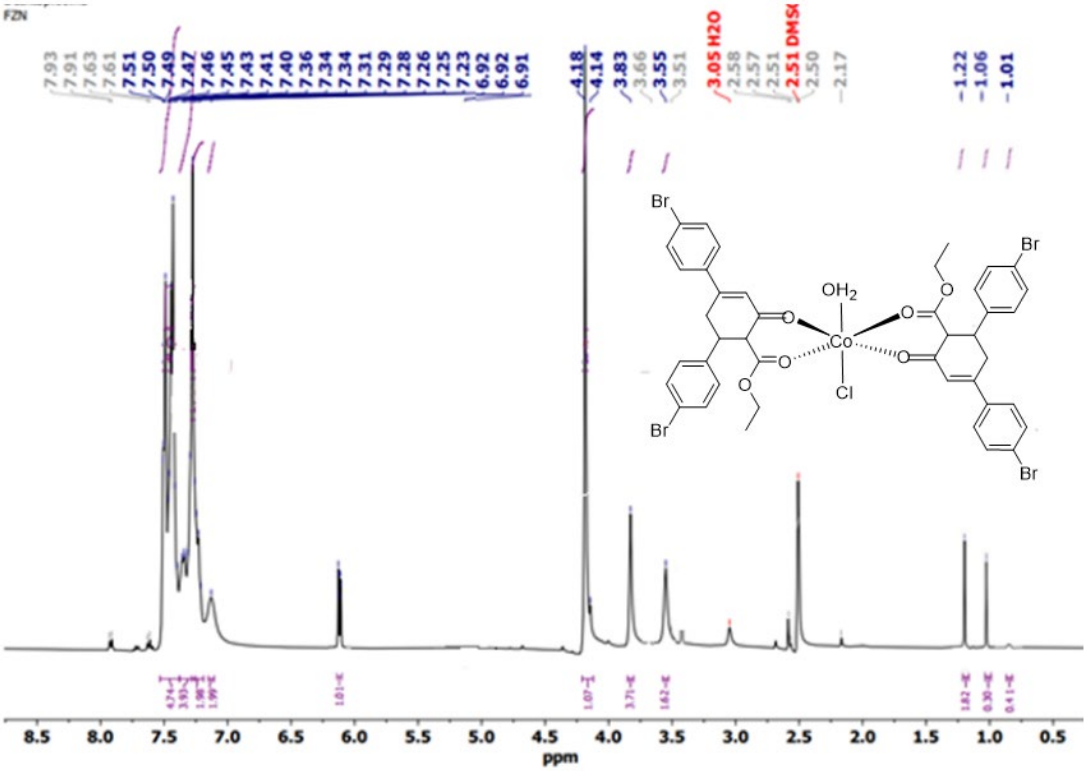

Figure 12. [1]HNMR spectrum of L2-Co.

3.5. Mass spectrometry of L1, L2 and its complexes

The synthesized ligands L1 and L2 have been described using mass spectrometry by examining their fragmentation ions. The mass spectrum displayed low to moderate peaks for the molecular ions of L1 and L2 in **Figures 13** and **14**. The main peaks of the molecular ion of L1 were observed at 449.3 m/z and 477.8 m/z, respectively, which are attributed to the (M + H) ions, confirming the calculated molecular weights of L1 and L2. The additional signals observed in the spectra are attributed to expected fragmentation patterns, at 159m/z which refer to C6H5Br Fragmentation also another peak at 136 m/z which attributed to cyclohexenon ring substituted with two methyl groups.

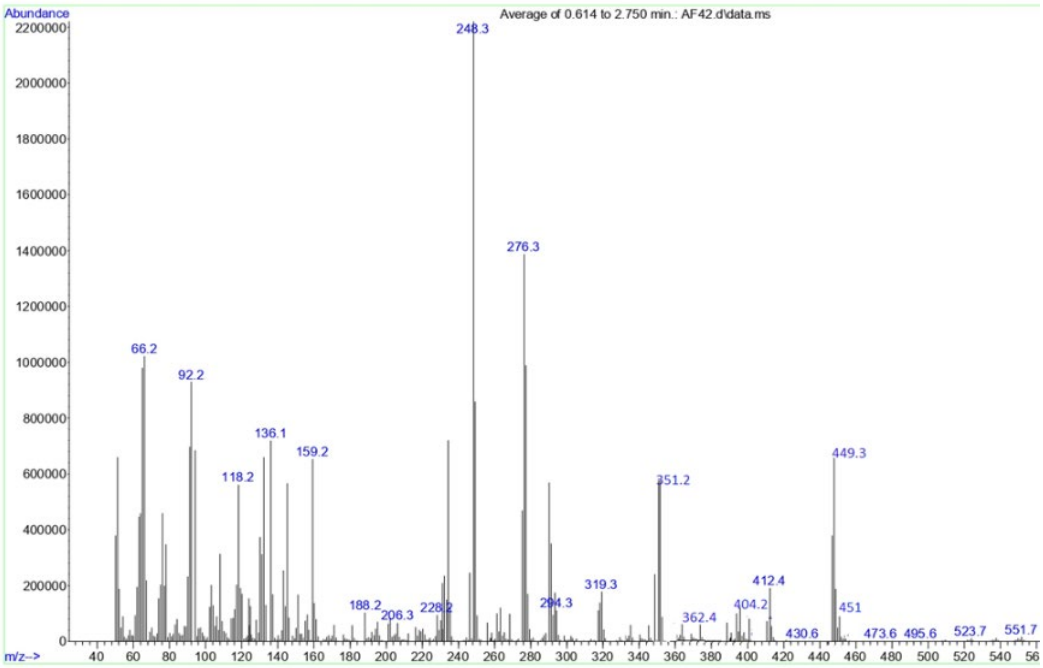

Figure 13. Mass spectrum of L1.

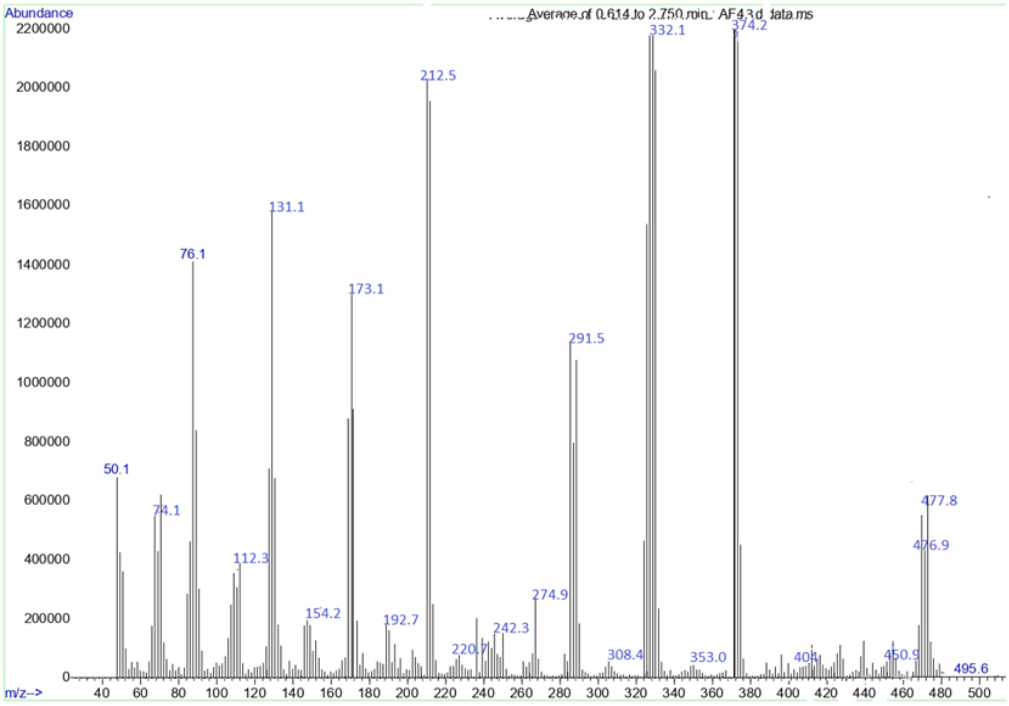

Figure 14. Mass spectrum of L2.

3.6. The efficiency of Fungi

The ability to resist of a preparation of ligands and their complexes to a specific kind of fungus (C. albicans) was investigated. Within 24 hours at 37°C, the samples are dissolved in dimethyl sulfoxide to reach the final concentration of (10^{-3}) mg/ml. **Table 4** and **Figure 15** illustrate the effectiveness of the fungi-resistant data assessed compounds, which shows the fungicidal ability of the new ligands and their complexes against the fungus under investigation (C. albicans). From the data and involvement in the Table, the dependent main points are deduced:

1. [L1] *and* [L2] ligands showed efficient resistance (C. albicans)[15].

2. All the ligands [L1] and [L2] complexes presented efficient resistance (C. albicans)[16].

3. Copper complex for ligand [L1] offered a higher efficiency contrast with the other complexes[17,18].

Table 4. The efficiency of Fungi (C. albicans) for ligands [L1], [L2], and their complexes.

No.	Compounds	*C.albicans*
	DMSO	-
	L1	11
	[Cr ($C_{20}H_{18}Br_2O_2$)$_2$ (H_2O)$_2$]Cl	14
	[Cu ($C_{21}H_{19}BrO_3$)$_2$ (H2O)$_2$]	16
	L2	12
	[Co ($C_{21}H_{19}BrO_3$)$_2$ Cl_2]	15
	[Ni ($C_{21}H_{19}BrO_3$)$_2$ Cl_2]	14

C. albicans= Candida albicans

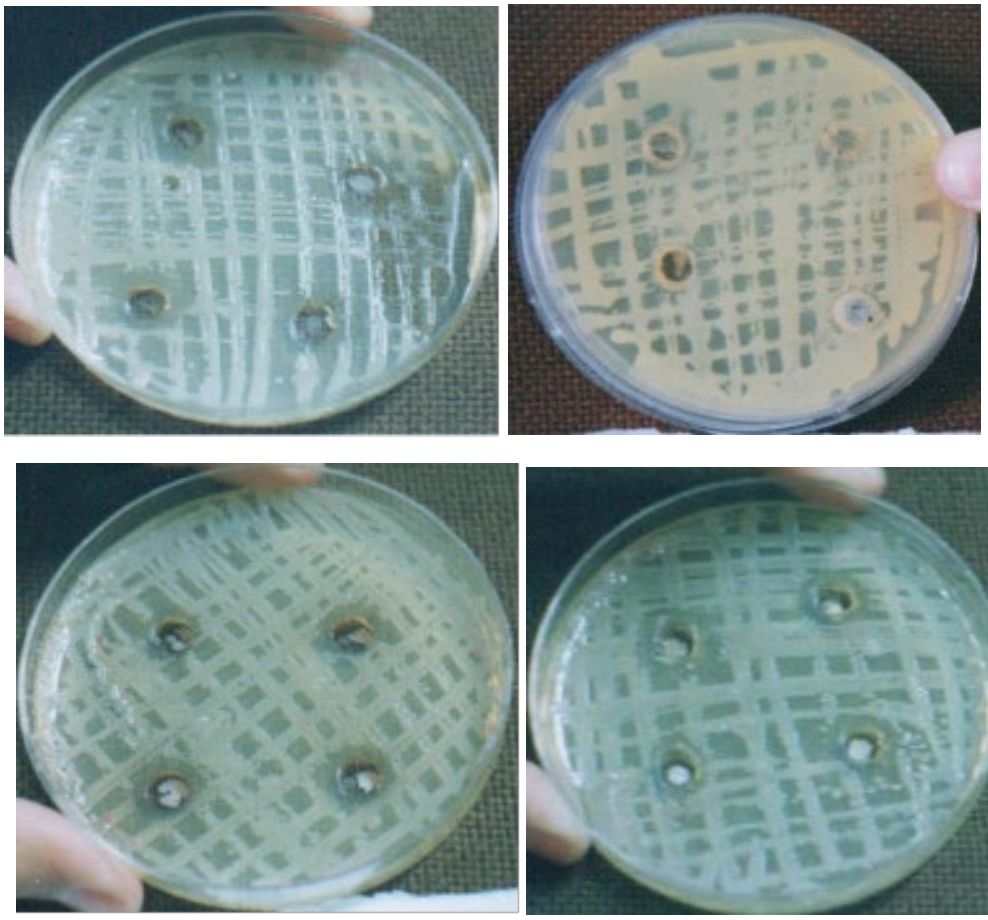

Figure 15. Antibacterial activity for ligand L1, L2, and their complexes.

3.7. Density frontier theory

The electronic properties of the compounds were explained by the frontier molecular orbitals (FMOs). The highest occupied molecular orbital (HOMO) and the lowest unoccupied molecular orbital (LUMO) were examined to understand the compound's chemical reactivity and potential applications. The FMO orbitals, as represented in **Figure 16**, and the color scheme of the HOMO and LUMO orbitals are essential for understanding their behavior. The colors help chemists visualize the energy distribution of the orbitals. The red color illustrates higher energy electrons, and the blue color represents lower energy electrons. Predicting

chemical properties and reactivity is essential for understanding the energy levels of electrons in a given atom or molecule[19].

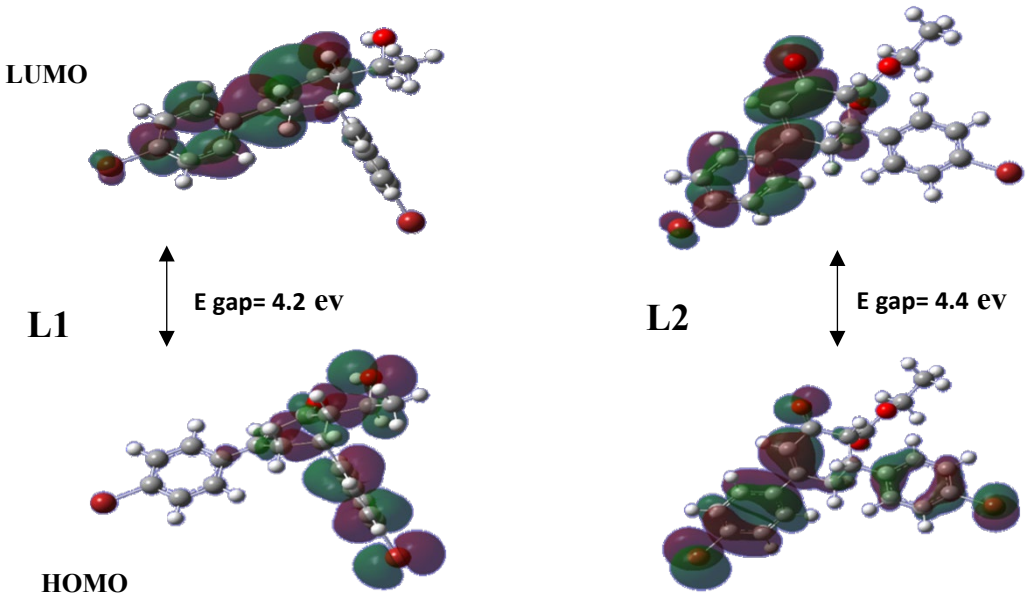

Figure 16. HÕMO and LUMÕ plots for L1, L2 using DFT/B3LYP.

For the optimized structures, the HOMO localization on certain groups is important to note. In particular, the highest negative region localized is distributed over the (O) O-H, and (O) C=O groups. This observation may have implications when considering the key location for nucleophilic attack at the core metal ion. While the maximum positive potentiality of LUMO orbitals is distributed over almost the entire molecule, this suggests that the molecule may have a higher tendency to interact with other molecules or participate in chemical reactions. The HOMO–LUMO energy gap is a key indicator of the physical and chemical properties of molecules. A greater degree of hardness, less polarizability, greater chemical stability, and decreased reactivity have all been linked to a greater energy difference between the highest occupied molecular orbital (HOMO) and lowest unoccupied molecular orbital (LUMO)[20,22]. The energy gap between HOMO and LUMO of L1, L2 is calculated by the DFT method and the B3LYP level, which are given in **Table 5**. The relatively large LUMO-HOMO energy gap of L2 (4.4 eV) indicates that it can be considered kinetically stable; however, L1 has the lowest HOMO-LUMO energy gap (4.2 eV), implying that it has the worst kinetic stability. In addition, molecules with low-lying LUMO orbitals tend to be more reactive than those with high-lying LUMO orbitals; therefore, L2 is more stable than L1. This suggests that compounds with large HOMO–LUMO energy gaps are more chemically stable than those with smaller gaps.

Table 5. The energy gap in eV of the ligands using the B3LYP method and the 3-21G basis set.

Compound	E HOMO	E LUMO	E gap
L1	-6.64	-2.44	4.2
L2	-6.52	-2.08	4.4
[CrL1]	-4.12	-2.58	1.53
[CuL1]	-8.43	-6.67	1.76
[NiL2]	-8.42	-5.21	3.21
[CoL2]	-8.34	-5.51	2.83

The HOMO-LUMO of L1 and L2 complexes are presented in **Figures 16** and **17**. Complexes 1-4 have a smaller energy gap (1.53, 1.76, and 3.21 eV, and 2.83, respectively) compared to L1, L2, **Table 5**. Interestingly,

complexes with narrow gaps exhibit higher reactivity compared to their equivalent ligands. This is due to their ease of providing acceptors with electrons. This comparison can shed light on the role of the ligands in influencing the activity of the complexes, further enhancing our understanding of their overall functionality. The reactive sites of the complexes can be further explored to understand their behavior. For the complexes of L1, the delocalization of the HOMO density on the Cr cation is across the ligand π-system and some of the metal contribution, while the LUMO density shows potential π→π* nature. While the HOMO density of the Cu complex shows a strong contribution near the copper center mixing with ligand orbitals, the delocalization appears over the ligand for the LUMO density. In Ligand 2 complexes, the HOMO density of the nickel complex is localized mainly on the π ligand framework, while the LUMO is ligand-metal charge transfer. The HOMO of the Co complex is mainly localized around the Co atom and oxygen donor atoms; in contrast, the LUMO density is primarily delocalized over the ligand framework, especially on the benzene ring.

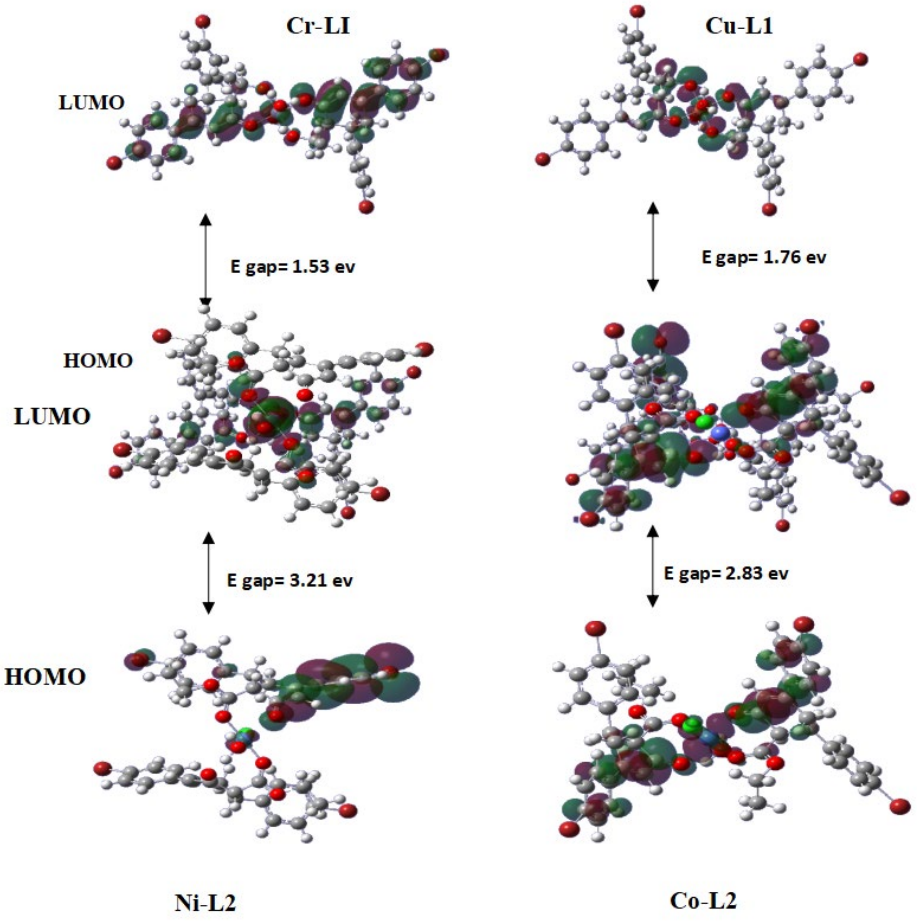

Figure 17. HOMO and LUMO plots of complexes using DFT/B3LYP.

3.8. Molecular Orbital Properties

The energies obtained from the frontier molecular orbitals of HOMO and LUMO have proved important universal concepts in quantum chemical calculations. In particular, valuable information regarding ionization potential (IP), electron affinity (EA), electronegativity (χ), electrophilicity index (ω), hardness (η), softness(s), and chemical potential (μ) have been deduced from the method, which provides an accurate and reliable framework for measuring the extent of chemical reactivity in molecular complexes.

Table 6 illustrates the chemical properties of ligands and their complexes. A molecule with a large HOMO-LUMO gap is generally harder and more stable; on the other hand, a small HOMO-LUMO gap is considered a soft molecule and less chemically stable[23]. Thus, low-energy gap molecules would be highly reactive and polarizable, while those with a high energy gap value would be less reactive and less polarizable.

The values of ionization potential (IP) and electron affinity (EA) of ligands and their corresponding complexes highlight their stability and redox behavior[24]. According to Table 6, the IP values are around 6.5 eV, and the EA is close to 2 eV for free ligands, suggesting their relative stability and resistance to redox processes. In the case of metal complexes, there are some variations observed in these properties. As an example, there is a decrease in the IP value of Cr-L1 with a difference of 4.1 eV, making electron extraction easier compared to the free form and thus facilitating oxidation. In contrast, copper and nickel, and cobalt complexes with ligand 1 and ligand 2, respectively, show high values for both IP and EA values with a range between 6 to 8 eV. This shows their strong electron-accepting tendency and high stabilization of their frontier orbitals. This shift in electron density upon complexation directly impacts how readily the electron transfer process occurs. The hardness values of free ligands were found in between 2.1 to 2.2 eV. These values categorize them as moderately challenging species that resist distortion of their electron density. In contrast, the Cr–L1 complex was found to be much softer, with a low hardness value of only 0.77 eV and a corresponding softness of 1.3, reflecting their strong polarizability and thus greater chemical reactivity. The copper, cobalt, and nickel complexes exhibit an intermediate range, with hardness values ranging from approximately 0.9 to 1.6 eV. They are relatively softer compared to the ligands but less reactive than the chromium complex. Generally, softer complexes exhibit greater chemical reactivity and show improved charge transfer interactions. Electronegativity (χ) and chemical potential (μ) further provide insight into the electron-attracting capability of these complexes. The free ligands possess moderate electronegativity values ranging between 4.3 and 4.5 eV. In contrast, the Cr–L1 complex value drops to a much lower electronegativity value, approximately 3.35 eV, revealing its low electron affinity.

In summary, free ligands exhibit relatively more complexity and maintain their reactivity. Upon complexation, a decrease in hardness generally occurs, thereby making the system softer, enhancing its polarizability, and increasing its reactivity. The chromium complex demonstrates exceptionally softness and reactivity but less stability. The copper complex, by contrast, is highly electrophilic and an efficient electron acceptor, achieving stability after charge acceptance. The nickel and cobalt complexes represent an intermediate position, softer than the free ligands and efficient electron acceptors, thus balancing reactivity and stability.

Table 6. Calculated global reactivity descriptors of ligands using the DFT/B3LYP method.

Parameter	formula	L1	L2	[Cr L1]	[Cu L1]	[Ni L2]	[CoL2]
I.P. (eV) Ionization energy	$-E_{HOMO}$	6.64	6.52	4.12	8.43	8.42	8.34
E.A(eV) Affinity	$-E_{LUMO}$	2.44	2.08	2.58	6.67	5.21	5.51
Electronegativity χ (eV)	(IP+EA)/2	4.54	4.30	3.35	7.55	6.82	6.94
Chemical potential μ (eV)	$-\chi$	-4.54	-4.30	−3.35	−7.55	–6.82	-6.94
Global electrophilicity index ω (eV)	$\mu^2/2\eta$	4.91	4.16	7.29	32.4	14.45	16.91
Softness S (eV^{-1})	$1/2\eta$	0.476	0.450	1.30	1.14	0.621	0.71
Hardness η (eV)	(IP – EA)/2	2.10	2.22	0.77	0.88	1.61	1.42

3.9. Molecular electrostatic potential surface

Molecular electrostatic potential analysis provides a powerful insight into the reactivity trends of molecules and interaction tendencies. The approach relies on mapping electronic density in a molecule to identify the electrophilic or nucleophilic attack. The corresponding three-dimensional potential map is depicted as a color-coded energy surface, with blue representing the most positive values and red representing the most negative[25,26]. As shown in **Figure 18**, plotting the distribution of electrostatic potential across a molecular surface reveal that the negative potential regions are predominantly localized around the electronegative atoms, particularly oxygen atoms. Conversely, the positive potential regions surround the hydrogen atoms. This trend

is consistent with our expectations, as electronegative atoms have a stronger pullon electrons and will thus generate more negative potential. In contrast, hydrogen, with its lone electron, will have a higher positive potential.

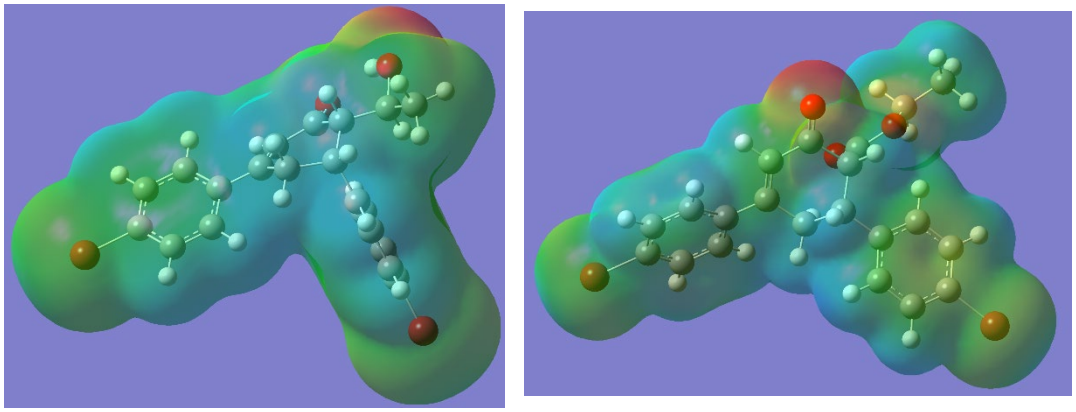

Figure 18. Molecular electrostatic potential diagram of ligands.

4. Conclusion

Based on the findings of 1H NMR, LC-MS, UV-Vis, magnetic moment, molar conductivity, and biological activity assessment for the ligand and corresponding complexes, the configuration of ligands L1 and L2 were verified. The proposed geometry of the generated compounds was octahedral, and they exhibited non-electrolyte properties for the Cu-L1, Co-L2, and Ni-L2 complexes, while the Cr-L1 complex had electrolyte properties. Every creative molecule exhibits biological activity against the fungal species (C. albicans). The produced compounds may have pharmaceutical properties. The calculated geometric parameters using DFT at the B3LYP/3-21 level revealed that the HOMO–LUMO energy gap of ligands is higher than their complexes. Additionally, the UV–Vis analysis was further assigned via TD-DFT at the B3LYP level, and the predicted results yield a good agreement with the experimental findings.

Acknowledgments

We are thankful of the facilities and laboratories provided by the Department of Chemistry, College of Science, Mustansiriyah University.

Conflict of interest

The authors declare no conflict of interest.

References

1. Badshah A, Nazar MF, Mahmood A, Ahmed W, Abdullah MI, Zafar MN, et al. Synthesis, characterization of novel cyclohexenone derivatives, and computation of their optical response. J Mol Struct. 2014;1071: 103–10.
2. Yang YQ, Chai Z, Wang HF, Chen XK, Cui HF, Zheng CW, et al. Chiral primary-secondary diamines catalyzed Michael-aldol-dehydration reaction between benzoylacetates and α,β-unsaturated ketones: Highly enantioselective synthesis of functional chiral cyclohexenones. Chemistry - A European Journal. 2009;15(48):13295–8.
3. Senguttuvan S, Nagarajan S. A simple and practical method for the synthesis of 2-amino-5, 6-dihydro-5, 7-diarylquinazolin-4-ols. J Heterocycl Chem. 2009;46(6):1346–8.
4. Padmavathi V, Reddy BJM, Balaiah A, Reddy KV, Reddy DB. Synthesis of some fused pyrazoles and isoxazoles. Molecules. 2000;5(12):1281–6.
5. Harrison WTA, Mayekar AN, Yathirajan HS, Narayana B, Sarojini BK. Ethyl 4-(2, 4-dichlorophenyl)-6-(6-methoxy-2-naphthyl)-2-oxocyclohex-3-ene-1-carboxylate. Structure Reports. 2010;66(10):o2478–o2478.
6. Zhang C, Qi JF, Cui DM, Wang Q, Wang XL. Platinum-catalyzed hydrative cyclization of 1,6-diynes for the synthesis of 3,5-substituted conjugated cyclohexenones. Molecules. 2010;15(7):5045–52.
7. Mayekar AN, Li H, Yathirajan HS, Narayana B, Kumari NS. Synthesis, characterization, and antimicrobial study of some new cyclohexenone derivatives. Int J Chem. 2010;2(2):114.

8. Ahmed RI, Osman EEA, Awadallah FM, El-Moghazy SM. Design, synthesis, and molecular docking of novel diarylcyclohexenone and diarylindazole derivatives as tubulin polymerization inhibitors. J Enzyme Inhib Med Chem. 2017;32(1):176–88.
9. Frisch MJ, Trucks GW, Schlegel HB, Scuseria GE, Robb MA, Cheeseman JR, Scalmani G, Barone V, Petersson GA, Nakatsuji H, Li X. Gaussian 16, revision a. 03, gaussian, inc., wallingford ct. Gaussian16 (Revision A. 03). 2016
10. Yusuf TL, Oladipo SD, Zamisa S, Kumalo HM, Lawal IA, Lawal MM, et al. Design of new Schiff-Base Copper (II) complexes: Synthesis, crystal structures, DFT study, and binding potency toward cytochrome P450 3A4. ACS Omega. 2021;6(21):13704–18.
11. Al-Fakeh MS, Alsikhan MA, Alnawmasi JS. Physico-chemical study of Mn (II), Co (II), Cu (II), Cr (III), and Pd (II) complexes with Schiff-base and aminopyrimidyl derivatives and anti-cancer, antioxidant, antimicrobial applications. Molecules. 2023;28(6):2555.
12. El-Ghamry MA, Elzawawi FM, Aziz AAA, Nassir KM, Abu-El-Wafa SM. New Schiff base ligand and its novel Cr (III), Mn (II), Co (II), Ni (II), Cu (II), Zn (II) complexes: Spectral investigation, biological applications, and semiconducting properties. Sci Rep. 2022;12(1):17942.
13. Sunjuk M, Al-Najjar L, Shtaiwi M, El-Eswed B, Al-Noaimi M, Al-Essa L, et al. Transition metal complexes of Schiff base ligands prepared from reaction of aminobenzothiazole with benzaldehydes. Inorganics (Basel). 2022;10(4):43.
14. Lever ABP, Rice SA. Inorganic electronic spectroscopy. American Institute of Physics; 1969.
15. Alghool S, Abd El-Halim HF, Dahshan A. Synthesis, spectroscopic, thermal, and biological activity studies on azo-containing Schiff base dye and its Cobalt (II), Chromium (III), and Strontium (II) complexes. J Mol Struct. 2010;983(1–3):32–8.
16. Al-Alzawi SM, Al-Jibouri MN, Rasheed AM, Al-Bayati SM. Synthesis, characterization, and antimicrobial activity of complexes of metal ions Ni (II), Zn (II), Pd (II), and Pt (IV) with polydentate 1, 2, 4-triazole ligand. Indonesian Journal of Chemistry. 2023;23(1):210–8.
17. Al-Assafe AY, Al-Quaba RAMS. New series of Ni (II), Cu (II), Zr (IV), Ag (I), and Cd (II) complexes of trimethoprim and diamine ligands: Synthesis, characterization, and biological studies. Indonesian Journal of Chemistry. 2024;24(3):812–21.
18. Khamees NM, Ahmed YJ, Al-Bayati S, Alazawi S, Rasheed A. Synthesis, characterization, and bioactive evaluation of cobalt (II) and copper (II) complexes of {4-[5-(5-sulfanylidene-2, 5-dihydro-1H-1, 2, 4-triazol-3-yl) furan-2-yl] phenyl} acetic acid. Bull Chem Soc Ethiop. 2024;38(6):1595–607.
19. Becke AD. A new mixing of Hartree-Fock and local density-functional theories. Journal of chemical Physics. 1993 Jan;98(2):1372-7.
20. Shahab H, Husain Y. Theoretical Study for Chemical Reactivity Descriptors of Tetrathiafulvalene in gas phase and solvent phases based on Density Functional Theory. Passer Journal of Basic and Applied Sciences. 2021 Sep 1;3(2):167-73.
21. Sharmila S, Mahalakshmi C. Homo Lumo Study, Reactivity Descriptors and Mulliken Charges of Imidazole Derivative. IRJEdT. 2023;5(4):35-8.
22. Miar M, Shiroudi A, Pourshamsian K, Oliaey AR, Hatamjafari F. Theoretical investigations on the HOMO–LUMO gap and global reactivity descriptor studies, natural bond orbital, and nucleus-independent chemical shifts analyses of 3-phenylbenzo [d] thiazole-2 (3 H)-imine and its para-substituted derivatives: Solvent and substituent effects. Journal of Chemical Research. 2021 Jan;45(1-2):147-58.
23. Hekim S, Azeez YH, Akpinar S. The theoretical investigation of the HOMO, LUMO energies and chemical reactivity of C9H12 and C7F3NH5Cl molecules. Journal of Physical Chemistry and Functional Materials. 2019;2(1):29-31.
24. Choudhary V, Bhatt A, Dash D, Sharma N. DFT calculations on molecular structures, HOMO–LUMO study, reactivity descriptors and spectral analyses of newly synthesized diorganotin (IV) 2-chloridophenylacetohydroxamate complexes. Journal of computational chemistry. 2019 Oct 15;40(27):2354-63
25. Demircioğlu Z, Kaştaş G, Kaştaş ÇA, Frank R. Spectroscopic, XRD, Hirshfeld surface and DFT approach (chemical activity, ECT, NBO, FFA, NLO, MEP, NPA& MPA) of (E)-4-bromo-2-[(4-bromophenylimino) methyl]-6-ethoxyphenol. Journal of Molecular Structure. 2019 Sep 5;1191: 129-37.
26. Albayati MR, Kansız S, Dege N, Kaya S, Marzouki R, Lgaz H, Salghi R, Ali IH, Alghamdi MM, Chung IM. Synthesis, crystal structure, Hirshfeld surface analysis and DFT calculations of 2-[(2, 3-dimethylphenyl) amino]-N'-[(E)-thiophen-2-ylmethylidene] benzohydrazide. Journal of Molecular, 2020, 1205, 127654.